



Picornaviral polymerase domain exchanges reveal a modular basis for distinct biochemical activities of viral RNA-dependent RNA polymerases

Colleen Watkins, Brian Kempf, Stéphanie Beaucourt, David Barton, Olve Peersen

► To cite this version:

Colleen Watkins, Brian Kempf, Stéphanie Beaucourt, David Barton, Olve Peersen. Picornaviral polymerase domain exchanges reveal a modular basis for distinct biochemical activities of viral RNA-dependent RNA polymerases. *Journal of Biological Chemistry*, 2020, 295 (31), pp.10624-10637. 10.1074/jbc.RA120.013906 . pasteur-03216660

HAL Id: pasteur-03216660

<https://pasteur.hal.science/pasteur-03216660>

Submitted on 4 May 2021

HAL is a multi-disciplinary open access archive for the deposit and dissemination of scientific research documents, whether they are published or not. The documents may come from teaching and research institutions in France or abroad, or from public or private research centers.

L'archive ouverte pluridisciplinaire **HAL**, est destinée au dépôt et à la diffusion de documents scientifiques de niveau recherche, publiés ou non, émanant des établissements d'enseignement et de recherche français ou étrangers, des laboratoires publics ou privés.



Distributed under a Creative Commons Attribution 4.0 International License



Picornaviral polymerase domain exchanges reveal a modular basis for distinct biochemical activities of viral RNA-dependent RNA polymerases

Received for publication, April 16, 2020, and in revised form, May 28, 2020. Published, Papers in Press, June 3, 2020. DOI 10.1074/jbc.RA120.013906

Colleen L. Watkins¹, Brian J. Kempf², Stéphanie Beaucourt³ , David J. Barton², and Olve B. Peersen^{1,*}

From the ¹Department of Biochemistry and Molecular Biology, Colorado State University, Fort Collins, Colorado, USA, the

²Department of Immunology and Microbiology, University of Colorado School of Medicine, Aurora, Colorado, USA, and the

³Institut Pasteur, CNRS UMR 3569, Paris, France

Edited by Karin Musier-Forsyth

Picornaviral RNA-dependent RNA polymerases (RdRPs) have low replication fidelity that is essential for viral fitness and evolution. Their global fold consists of the classical “cupped right hand” structure with palm, fingers, and thumb domains, and these RdRPs also possess a unique contact between the fingers and thumb domains. This interaction restricts movements of the fingers, and RdRPs use a subtle conformational change within the palm domain to close their active sites for catalysis. We have previously shown that this core RdRP structure and mechanism provide a platform for polymerases to fine-tune replication rates and fidelity to optimize virus fitness. Here, we further elucidated the structural basis for differences in replication rates and fidelity among different viruses by generating chimeric RdRPs from poliovirus and coxsackievirus B3. We designed these chimeric polymerases by exchanging the fingers, pinky finger, or thumb domains. The results of biochemical, rapid-quench, and stopped-flow assays revealed that differences in biochemical activity map to individual modular domains of this polymerase. We found that the pinky finger subdomain is a major regulator of initiation and that the palm domain is the major determinant of catalytic rate and nucleotide discrimination. We further noted that thumb domain interactions with product RNA regulate translocation and that the palm and thumb domains coordinately control elongation complex stability. Several RdRP chimeras supported the growth of infectious poliovirus, providing insights into enterovirus species-specific protein–protein interactions required for virus replication.

Picornaviruses are a family of positive-strand RNA viruses responsible for a multitude of human and animal diseases. Upon infection, their 7.5-kb RNA genomes are directly translated via an internal ribosome entry site, yielding a ~250-kDa polyprotein that is cleaved into approximately a dozen individual proteins and multiple functional intermediates. RNA genome replication is carried out by the 3D^{pol} protein, a RNA-dependent RNA polymerase (RdRP) that first uses the infecting RNA as a template for making negative-strand RNA and then uses these as templates for generating new positive-strand RNA for translation or for packaging into progeny virus particles. The ≈460-residue picornaviral 3D^{pol} enzymes are among the smallest viral RdRPs, yet their core structure and mecha-

nism are retained in larger enzymes from other positive-strand RNA viruses (1–3), making them a useful model for studying RNA virus polymerase biochemistry.

The RdRP core structure has the classic polymerase resemblance to a cupped right hand with palm, fingers, and thumb domains. The palm domain contains conserved motifs A, B, and C that form the active site using the two-metal mechanism commonly found in replicative DNA polymerases (4), the finger domain binds template RNA, and the thumb domain interacts with dsRNA product. A notable and unique feature of positive-strand RNA virus RdRPs is that the fingers make direct contact with the top of the thumb domain, effectively encircling the active site and creating a short tunnel whereby NTPs enter the active site. Mutation of this interaction severely destabilizes poliovirus 3D^{pol} in thermal denaturation studies (5), leading to the theory that the viral RdRPs evolved the fingers–thumb contact to stabilize the fold of a small polymerase encoded within the space limitations of a small viral genome. This stabilization in turn has major implications for both nucleotide addition and translocation mechanisms.

Replicative polymerases often use a swinging motion of their fingers domain to capture and then position NTPs in the active site for catalysis, and these interactions play important roles in nucleotide recognition and replication fidelity (6, 7). The reverse motions to open the active site after catalysis facilitate translocation by directly contacting the RNA template and pushing it by one base-pair register in a power-stroke driven by pyrophosphate release (8). In contrast, positive-strand RNA virus RdRPs with their thumb-tethered fingers domain cannot undergo such motions, and they instead use a subtle movement of motifs A and D within the palm domain to fully structure the active site for chemistry only upon NTP binding (9, 10). Their fingers domains remain essentially stationary during the nucleotide addition cycle, and their mechanism for translocation is not yet well-understood beyond an initial half base-step product strand movement seen in enterovirus 71 polymerase structures (11).

This simple active-site closure mechanism gives rise to the relatively low replication fidelity that is a common feature of positive-strand RNA virus RdRPs, and it results in progeny virus populations composed of a large pool of sequence variants that are sometimes referred to as quasispecies (12–15). The population consensus sequence defines the virus, but close

*For correspondence: Olve B. Peersen, Olve.Peersen@ColoState.edu.

inspection of individual genomes show one or more random mutations relative to that consensus. This genetic diversity is essential for virus growth and spread, particularly in hosts in which the virus must replicate in a variety of cell types, and it has been shown that either increasing or decreasing polymerase fidelity will adversely affect virus growth (12, 16–18). To guard against hypermutation, RNA viruses also undergo recombination events whereby entire genome sections are swapped with counterparts from other viruses, allowing for the large-scale purging of deleterious mutations (19–22).

In a prior study of 3D^{pol} fidelity variants, we made the observation that despite having essentially identical structures, the poliovirus (PV) and coxsackievirus B3 (CV) enzymes differ drastically in their biochemical characteristics (23). PV 3D^{pol} elongates RNA 4-fold faster than CV 3D^{pol} with processive elongation rates of 88 *versus* 22 nucleotides/s at 37 °C, and it does so with much lower nucleotide discrimination than the CV enzyme. Interestingly, mutations in motif A tend to reduce CV 3D^{pol} fidelity, whereas analogous mutations in PV polymerase tend to increase fidelity. This led to the hypothesis that the picornaviral polymerases represent a minimal RdRP core structure whose biochemical characteristics can be easily fine-tuned by mutations and evolution to optimize the growth of any given virus. The strongest fidelity variants identified to date have been in the palm domain, near the active site or within structurally coupled motifs A and D, but some have also been identified in the fingers domain (1, 24). Both NMR data and molecular dynamics calculations implicate long range protein dynamics networks as modulators of fidelity (25–28). This led us to ask whether the different 3D^{pol} structural domains serve distinct and separable functions during the catalytic cycle, and the extent to which they can modulate each other's activity with respect to RNA replication functions. The project builds on prior work by Cornell and Semler (29) examining polyprotein processing and RNA-binding activities of chimeric poliovirus–coxsackievirus B3 3CD proteins, but with a focus on polymerase functions and a more detailed protein structure–driven approach.

In the work presented here, we use the high structural similarity of picornaviral polymerases to generate a set of chimeric enzymes that directly examine the role each polymerase structural domain plays in initiation, single cycle and processive elongation, translocation, elongation complex stability, and nucleotide discrimination. We also tested the ability of chimeric coxsackie–polio polymerases to support virus replication in cell culture.

Results

Chimeric polymerase design and purification

Polymerase domains for chimeric RdRPs were identified by inspection of superposed PV and CV 3D^{pol} structures (3, 30) and involve four distinct folding domains; the pinky finger sub-domain, the fingers domain, the palm domain, and the thumb domain (Fig. 1A). We name these chimeric polymerases using a four-letter code in the order pinky–fingers–palm–thumb, with the letter “C” or “P” denoting which virus (CV or PV) each domain was derived from. Thus, PPCC is a chimeric polymerase

with pinky and fingers domains from poliovirus and palm and thumb domains from coxsackievirus. The full set of chimeras generated are described under “Experimental procedures” with borders shown in Fig. 1B. The two WT proteins have 74% amino acid sequence identity and 86% similarity, and the CV enzyme is one residue longer because of a loop insertion at residue ~260 (Fig. 1B).

The chimeric polymerases generally expressed well in *Escherichia coli* and could be purified at high yield using the normal protocol of Ni-affinity, anion exchange, and size-exclusion chromatography followed by concentration to ~200 μM in 300 mM NaCl buffer. The one exception was the PPCC polymerase that had a tendency to aggregate upon concentration in high-salt buffer and during room-temperature initiation assays at micromolar concentrations in 75 mM salt, suggesting that its folding stability was compromised. This is not altogether unexpected considering the full fingers exchanges involve five different junction points inside an essentially contiguously folded domain boundary (Fig. 1B).

Initiation rates and elongation complex stability

Basic functionality was tested with RNA initiation assays that measure the time needed to form +1 RNA products after mixing polymerase with RNA and GTP, and with stability assays that provide a measure of stalled elongation complex lifetime. The initiation data were well fit by single exponential curves (Fig. 2, C and D), resulting in time constants that are dominated by a combination of RNA binding and a reorientation step that places the RNA into a catalytically competent conformation (Table 1). The WT PV (PPPP) and CV (CCCC) proteins have very different initiation times of 12 ± 2 and 1.4 ± 0.3 min, respectively. The data show this difference can almost entirely be attributed to the pinky finger structure; placing the CV pinky onto PV 3D^{pol} (CPPP) reduces initiation time from 12 to 2 min, and conversely placing the PV pinky on CV (PCCC) increases initiation time from 1.4 to 10 min. In contrast, swapping the entire fingers domains (CCPP and PPCC) leads to intermediate initiation times of 4 and 7 min, indicating that grafting the more extensive interdomain contacts between the palm and fingers domains disrupts but does not eliminate fingers domain function. Exchanging the thumb domains (PPPC and CCCP) had only minor effects on initiation rates.

The elongation complex stability assays test how much of the initiated RNA can be extended to full-length product after incubation in a high-salt buffer that prevents rebinding of RNA (Fig. 2); polymerase-bound RNA will be rapidly elongated to a +7 product, whereas dissociated RNA will remain as the +1 product. The WT elongation complexes are long-lived and inactivate with time constants of ~100 and ~150 min for PV and CV, respectively. All the chimeric polymerases form less stable complexes than their WT counterparts, with the smallest effects caused by the pinky swaps and the largest arising from the thumb swaps, but even the largest reductions of inactivation rate are less than 2-fold (Table 1). Notably, these experiments show that all the chimeric polymerases can form stable elongation complexes, enabling further biochemical analysis of nucleotide addition by rapid kinetics methods.

Modular functions of picornavirus polymerase domains

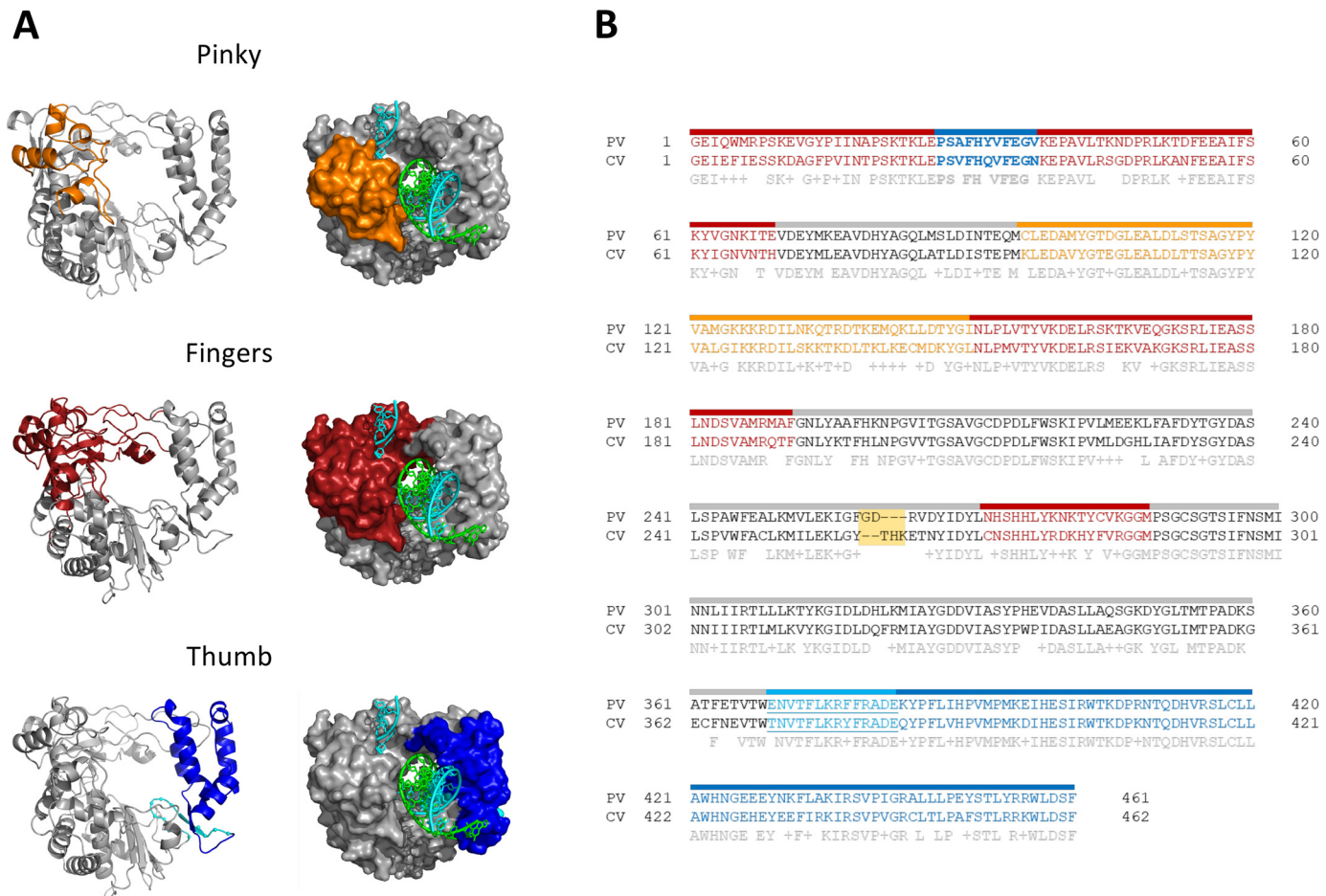


Figure 1. Chimeric polymerase construction. *A*, domain exchanges illustrated with the structure of 3D^{pol} elongation complex (Protein Data Bank entry 3OL6). The pinky finger is shown in orange, the entire fingers domain including the pinky finger is shown in red, and the thumb domain is shown in blue with the primer grip at the beginning of the thumb domain in light blue with α -carbon spheres. RNA is colored cyan for template and green for product strand. *B*, structure-based sequence alignment between poliovirus and coxsackievirus B3 polymerases to show the junction points used in the chimeric polymerase construction. Pinky, fingers, palm, and thumb domain colors correspond to those in *A*, with the palm domain sequence shown in gray. Residues 27–37 were considered as part of the thumb domain to preserve the fingers–thumb contact. There is 74% amino acid identity and 86% similarity between the two polymerases, and their structures are essentially identical except for a single-residue insertion in a loop at residue 260 (yellow box).

Rapid kinetics studies of elongation

Nucleotide incorporation kinetics were measured by stopped-flow fluorescence methods for processive elongation over a 20-nucleotide-long single-stranded RNA template (Fig. 3*A*) (31) and for a single nucleotide addition using CTP and 2'-deoxy-CTP (dCTP) templated by a guanosine (32) (Fig. 3*B*). The single cycle addition data were used to calculate a nucleotide discrimination factor as the ratio of the catalytic efficiencies for CTP and dCTP incorporation, *i.e.* $(k_{\text{pol}}/K_m)_{\text{CTP}}/(k_{\text{pol}}/K_m)_{\text{dCTP}}$. In this context we use k_{pol} to indicate a full nucleotide addition cycle (NAC) going from NTP binding through catalysis and translocation, at which point we observed changes in 2-aminopurine fluorescence. We have previously shown that the biochemical discrimination factor, which is rooted in the importance of the NTP 2'-OH group in stabilizing the closed conformation active site (9), serves as a proxy of changes to polymerase replication fidelity that correlated with mutation frequencies observed by genome sequencing methods (16, 23).

The data from the full set of chimeric polymerases are summarized in Fig. 4 as plots of nucleotide discrimination factors

versus the maximal processive elongation rates. The data from the pinky finger and complete fingers domain exchanges show a clear delineation of function in which the chimeric polymerases cluster by the origin of their palm and thumb domains (Fig. 4*A*). Exchanging the coxsackievirus pinky finger (CPPP) or full fingers domain (CCPP) onto PV 3D^{pol} has only minor effects on discrimination compared with the WT enzyme (PPPP), and this is also true for the converse PCCC versus CCCC pinky exchange. The PPCC protein was prone to aggregation, suggesting that its folding is compromised, and it is identified with *light gray* text in the figures.

The thumb domain exchanges, on the other hand, resulted in processive elongation rates and discrimination that were intermediates between those of the two WT enzymes (Fig. 4*B*). Placing the coxsackievirus thumb onto poliovirus polymerase (PPPC) decreased the processive elongation rate, and conversely placing the poliovirus thumb onto coxsackievirus polymerase (CCCC) increased the processive elongation rate. The single cycle elongation data using 2-aminopurine translocation as a reporter showed similar k_{pol} values of $\sim 28 \text{ s}^{-1}$

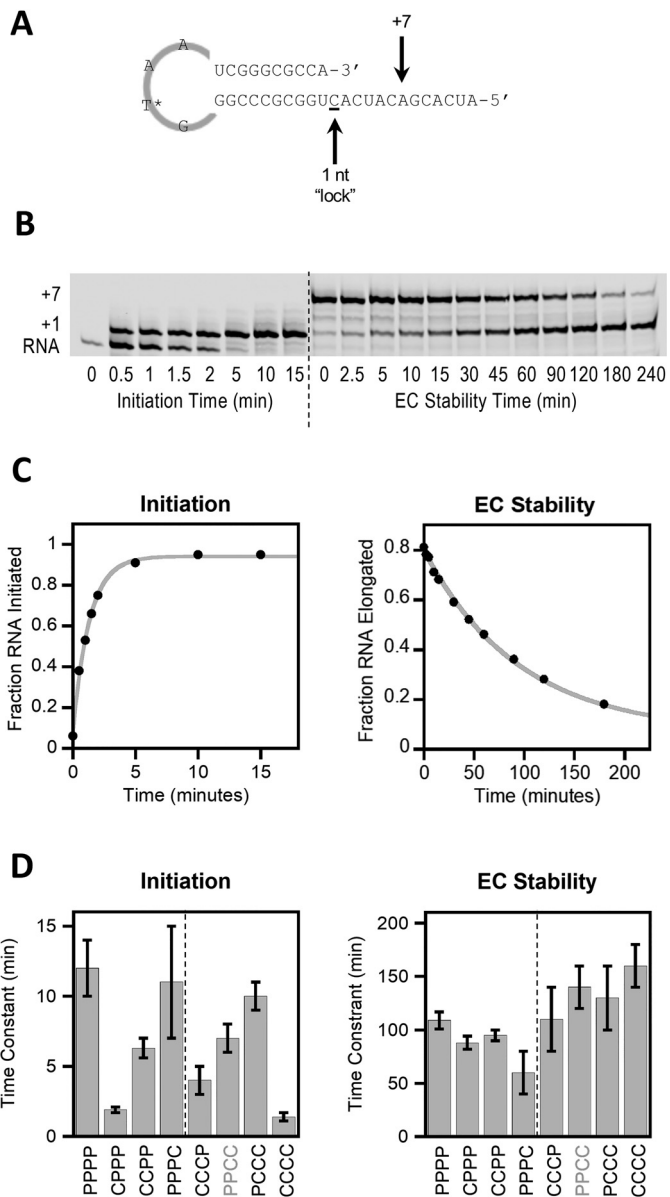


Figure 2. Polymerase initiation and stability. *A*, RNA construct used in initiation and stability assays. *B*, example gel used to quantitate RNA population changes with respect to time during the initiation and stability assays. Starting RNA, the +1 RNA product from a single GMP incorporation, and the +7 RNA product are labeled. The dashed vertical line denotes transition to the stability experiment in which +1 elongation complexes were assayed for their ability to chase to a longer +7 product upon addition of NTPs. Times are labeled with respect to the assay being conducted. *C*, example single exponential fitting used to determine time constants associated with initiation and elongation complex (EC) stability. *D*, results of the initiation and stability assays for the two WT (PPPP and CCCC) and six chimeric polymerases, grouped by polymerase palm domain with poliovirus on the left and coxsackievirus on the right of the dashed line. PPCC is shown in light gray to indicate that the protein is prone to aggregation in solution.

for the two thumb-exchanged enzymes, slightly elevated nucleotide K_m values compared with their parental palm and fingers domains, and nucleotide discrimination factors that were intermediate between those of either WT polymerase (Table 1). Note that the assays for the thumb exchanges were inadvertently done at pH 6.8 instead of 7.0, and this slightly reduces the discrimination factors for both WT and chimeric enzymes.

Rapid quench kinetics

The intermediate rates and discrimination factors observed for the thumb-exchange polymerases led us to further dissect their mechanism by rapid chemical quench methods to directly monitor RNA product formation. A single RNA substrate (Fig. 5A) was used for (i) chemical quench with EDTA to assay the NTP capture step, (ii) acid quench to assay the active-site closure and chemistry steps via product formation rates, and (iii) stopped-flow fluorescence to assay the overall NAC by reporting on the final translocation step (Fig. 5, B–D). The experiments were done at 30 °C with Bio-Logic QFM-4000 and SFS-4000 instruments that use the same syringe systems for reagent delivery. The resulting k_{obs} values were plotted against NTP concentration and fit to the equation $k_{obs} = k [NTP]/((k/(CE) + [NTP])$ to extract the catalytic efficiency, $CE \pm \sigma_{CE}$, and rate constant, $k \pm \sigma_k$, and their standard errors directly from the data (Table 2). Using the standard definition of CE as k/K_m then allows K_m values to be calculated as k/CE , with its error (σ_{Km}) obtained by standard root-mean-square error propagation.

Fitting these data generally required a double exponential function, of which only the faster phase showed NTP concentration dependence reflecting 70–80% of the observed amplitude. In a prior coxsackievirus 3D^{pol} study we also observed biphasic 2-aminopurine fluorescence data and attributed the constant phase to a slow ($k \approx 1 \text{ s}^{-1}$) final relaxation event within the post-translocation complex that slightly altered the 2-aminopurine environment (33). Here we now observed the same rate as a slow trailing phase of product formation in both the EDTA- and acid-quench experiments. Based on this, we conclude that this slower rate in fact represents a minor population of stalled elongation complexes that must undergo an initial slow transition event before becoming competent for NTP binding and catalysis, at which point they presumably progress through the NAC normally. The molecular nature of this event is not known, but it may be related to a conformational change step that occurs after RNA binding and before catalytic competence (34).

EDTA-quench derived rates that reflect nucleotide capture are very similar at 56 ± 3 and $59 \pm 5 \text{ s}^{-1}$ for the WT PV and CV enzymes (Table 2), and these values are not significantly altered by the thumb domain exchanges that yield rates of 56 ± 2 and 60 ± 4 for PPPC and CCCP, respectively. In contrast, the acid quench data show that elongation product formation occurs more slowly at rates of 42 ± 2 and $35 \pm 3 \text{ s}^{-1}$ for the WT PV and CV enzymes, respectively, and in this case both PPPC and CCCP thumb-exchanged enzymes have an intermediate rate of $\sim 37 \text{ s}^{-1}$. Thus, the CV thumb slows product formation by PV polymerase, and conversely the PV thumb accelerates product formation by CV polymerase. These observations are echoed and exacerbated in the translocation-dependent k_{2AP} values that reflect completion of the NAC; the PV polymerase rate is further slowed from 41 ± 4 to $31 \pm 3 \text{ s}^{-1}$, and the CV polymerase rate increases from 33 ± 4 to $38 \pm 5 \text{ s}^{-1}$.

The WT PV polymerase has higher catalytic efficiency than the CV enzyme in all three assays, which is primarily a reflection of higher-affinity nucleotide binding. This is most apparent in EDTA-quench data that are sensitive to the initial NTP

Modular functions of picornavirus polymerase domains

Table 1

Kinetic parameters of chimeric polymerases

3D ^{pol}	Initiation	Stability	Single nucleotide		Processive elongation		Discrimination factor
			k_{pol}	K_m	Rate	K_m	
PPPP (PV WT)	<i>min</i> 12 ± 2	<i>min</i> 109 ± 8	26 ± 1	30 ± 3	24 ± 1	105 ± 5	120 ± 20
CCCC (CV WT)	1.4 ± 0.3	160 ± 20	22 ± 1	35 ± 2	17 ± 1	153 ± 6	300 ± 20
Pinky exchanges							
CPPP	1.9 ± 0.2	88 ± 6	30 ± 1	42 ± 5	19 ± 1	76 ± 8	120 ± 20
PCCC	10 ± 1	130 ± 30	18 ± 1	45 ± 6	14 ± 1	120 ± 20	270 ± 20
Fingers exchanges							
CCPP	4 ± 1	95 ± 5	28 ± 1	32 ± 4	26 ± 1	83 ± 4	120 ± 20
PPCC	7 ± 1	140 ± 20	13 ± 1	60 ± 9	5 ± 1	101 ± 10	180 ± 20
Thumb exchanges							
PPPC	11 ± 4	60 ± 20	29 ± 2	37 ± 3	21 ± 1	148 ± 9	150 ± 20
CCCP	4 ± 1	110 ± 30	28 ± 1	52 ± 7	19 ± 1	147 ± 5	160 ± 20

capture event, in which the two polymerase efficiencies differ 1.6-fold, but the trend of higher PV efficiency is also observed in the acid-quench and 2-aminopurine fluorescence assays, in which the thumb exchange reduces the PPPC efficiencies to be comparable with those of the WT CV. These data indicate the biochemical functions of the palm and thumb domains are tightly coordinated to maximize the speed of the nucleotide addition cycle after the rate-limiting chemistry step.

Two-cycle elongation assays

To further investigate the different effects of palm and thumb domains on NAC rates, we carried out stopped-flow fluorescence studies with an RNA that was sensitive to two nucleotide incorporation steps (Fig. 6A). The 3D^{pol} elongation complex structures show that the downstream +3 base on the template strand is partially stacked on the further downstream +4 base, and as a result its fluorescence will be quenched compared with the fully unstacked +2 position (35). This allowed us to design an RNA wherein a 2-aminopurine would start in the low-fluorescence +3 site, transition through the high-fluorescence +2 site, and finally enter the low-fluorescence +1 site, in which elongation is effectively terminated by a lack of rapid nucleotide incorporation opposite the 2-aminopurine template. Initiation was done via the incorporation of a four-nucleotide GAGA sequence to generate stalled elongation complexes, and the stopped-flow fluorescence data reflect two sequential cytosine incorporation events. The data were analyzed using KinTek Explorer (KinTek Corp, Austin TX) (36, 37) with a double incorporation model in which two CTP-binding equilibria and two translocation rates were fit simultaneously. The explicit modeling of the full data sets also required inclusion of the slow activation step discussed above for a portion of the stalled elongation complexes, and it is this population that give rise to the slow trailing decrease observed in the fluorescence traces ($k \approx 1\text{s}^{-1}$). The fraction of total elongation complex in the initially “inactive” state represented 30–40% of the total 20 nm complex used in the reaction and was determined empirically for each data set because it varied for each initiation reaction.

Fig. 6B shows the data obtained from the two WT and two thumb-exchanged polymerases as the CTP concentration was

titrated from 6 μM (red trace) to 46 μM (purple trace). Each titration series data set was collected using the variable volume mixing capabilities of the SFM-4000 instrument in \sim 10 min from initial instrument loading, which helps maintain consistent signal amplitudes by minimizing decay of the stalled elongation complex during the experiment. A visual comparison of the data traces from the two WT polymerases shows that PV 3D^{pol} is faster than CV 3D^{pol}; at the highest CTP concentrations with near maximal rates, PV 3D^{pol} reaches peak fluorescence in \approx 60 ms *versus* the slower \approx 90 ms needed for CV 3D^{pol}. The thumb exchanges affect this rate, slowing PPPC relative to the WT PPPP enzyme and accelerating CCCP relative to CCCC (Fig. 6B). Fitting these data to a double elongation model yielded K_m and k_{pol} values for both nucleotide incorporation cycles (Fig. 6C). For all four polymerases, the second nucleotide incorporation was more efficient than the first, and this was primarily driven by 2–3-fold faster k_{pol} rates. WT PV was faster than WT CV polymerase with rates for the second event of 38s^{-1} *versus* 24s^{-1} , and exchanging the thumb domains essentially reversed this relationship, with PPPC slowing to 27s^{-1} while CCCP became faster at 32s^{-1} . The effects on CTP K_D values were relatively minor, ranging from 5 to 15 μM among all the constructs, and unlikely to have significant effects on elongation rates at millimolar physiological nucleotide concentrations. Last, the activation rates for the slow population of stalled elongation complexes ranged from 0.8 to 1.9s^{-1} . These changed slightly with the thumb exchanges and appear to be somewhat faster with the PV thumb, although that is not a definitive conclusion from this limited data set. We did also attempt to fit a more comprehensive kinetic model involving discrete nucleotide-binding, chemistry, and translocation steps using global fitting of the EDTA, acid quench, and fluorescence data sets described in Fig. 5, but could not get satisfactory convergence of all the kinetic parameters involved.

Infectious virus studies

We tested whether the domain-exchanged polymerases could support virus growth by inserting their coding sequence into both poliovirus and coxsackievirus genomes, generating viral RNA by T7 transcription, and transfecting that RNA into HeLa cells. We did not recover any virus using the coxsackievirus

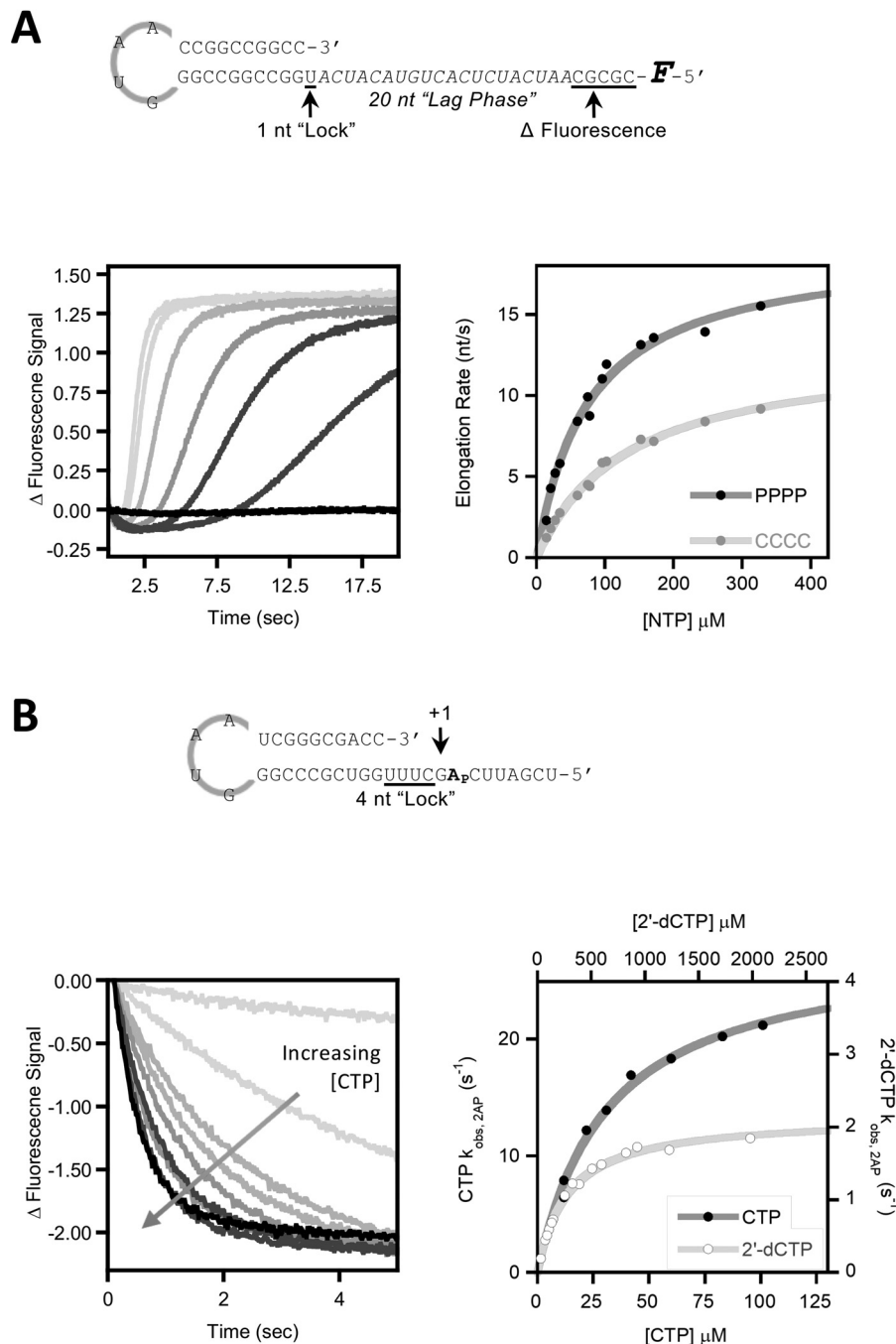


Figure 3. Elongation rate and nucleotide discrimination determination. *A*, RNA template used for processive elongation assay in which a single AMP incorporation was used to “lock” stalled elongation complexes prior to stopped-flow assays of processive elongation rates. The sample data at *left* show an NTP titration series in which the lag phase before the polymerase reaches and affects the 5'-fluorescein group shortens as NTP concentrations are increased, and the concentration dependence plot at *right* highlights the difference in processive elongation rates between poliovirus and coxsackievirus polymerases. *B*, RNA template designed for single CMP incorporation and nucleotide discrimination assay wherein a four-nucleotide “lock” for EC formation is done prior to using rapid stopped-flow fluorescence to monitor the translocation of the internal 2AP base following incorporation of a single cytosine base at different concentrations. The *right panel* is a double-XY plot showing concentration dependence of rates for both CTP (dark gray) and 2'-dCTP (light gray) substrates.

background, but in the poliovirus background we recovered infectious virus from both the pinky finger (CPPP) and full-fingers (CCPP) domain-exchanged polymerases (Fig. 7A). The titers of virus from the initial RNA transfections were ~ 10 -100-fold lower than those of the WT virus (5×10^5 to 10^6 versus 10^8 PFU/ml), but upon subsequent reinfection the domain-exchanged viruses replicated as well as WT poliovi-

rus. Sequencing showed the chimeric polymerase constructs were genetically stable without any additional mutations arising within their 3CD polyprotein regions.

To address the possibility that the domain exchange with the coxsackievirus thumb prevented virus replication by disrupting a known interaction between the PV palm and thumb domains (see “Discussion”), we made two mutations in the PPPC

Modular functions of picornavirus polymerase domains

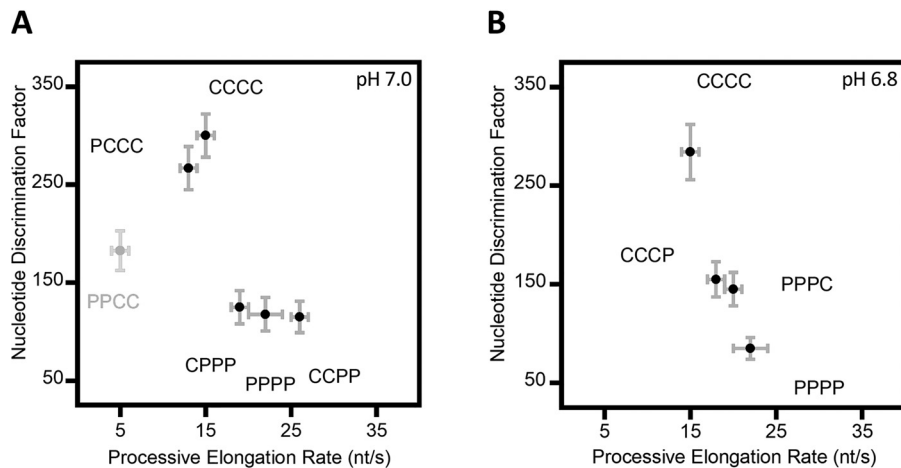


Figure 4. Nucleotide discrimination factor versus processive elongation rate plots. *A*, pinky and full fingers exchanges showing that the chimeric polymerases cluster according to their palm domains. The PPCC construct is shown in gray to reflect that it is an unstable protein that is prone to aggregation. *B*, data from the two thumb exchange polymerases showing elongation rates and nucleotide discrimination factors that are intermediate between the two WT enzymes.

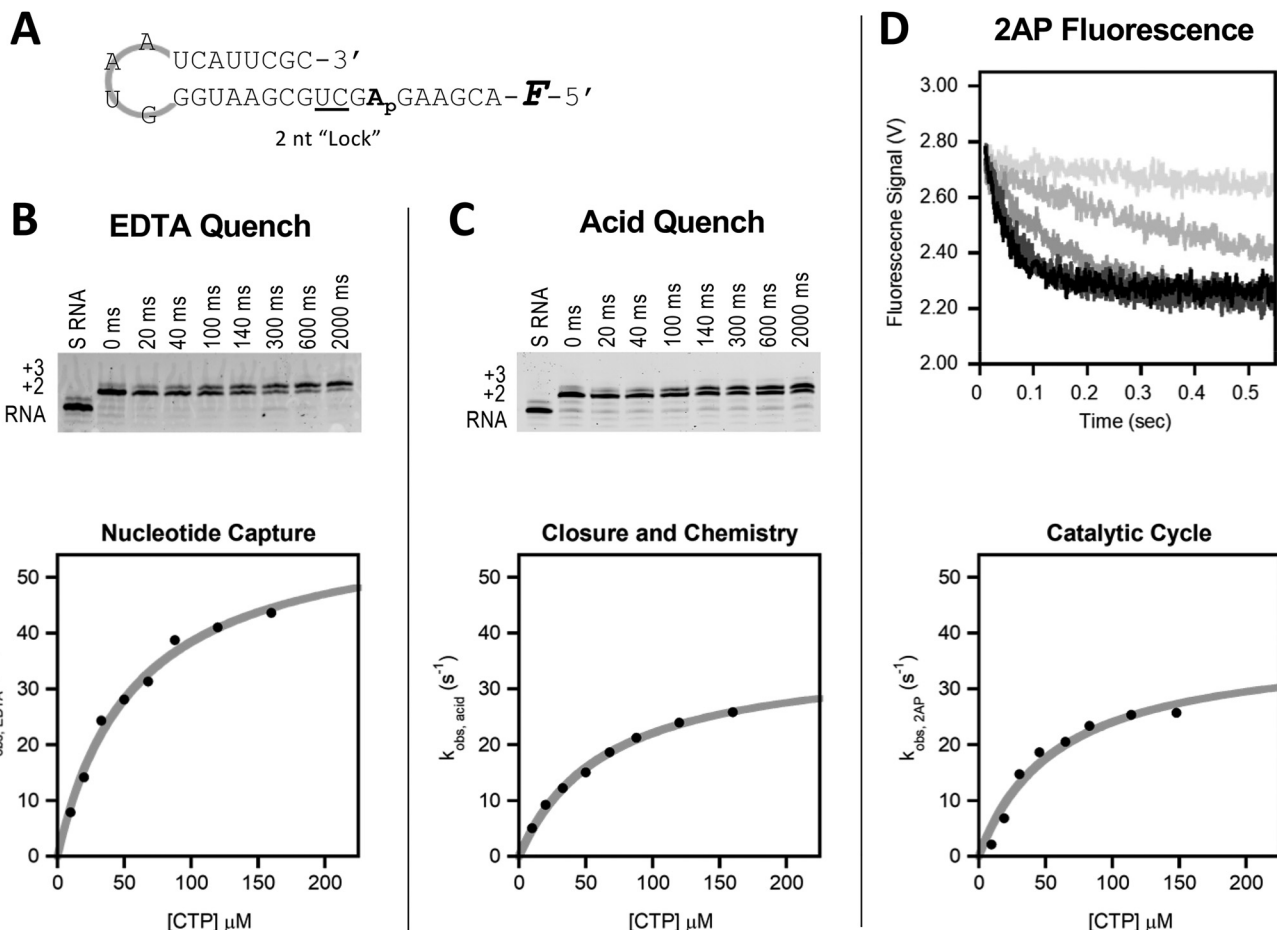


Figure 5. Rate and catalytic efficiency determination for individual steps of nucleotide addition cycle. *A*, RNA hairpin construct used for rapid chemical quench and stopped-flow experiments. Briefly, stable EC was formed using a two-nucleotide "lock," the 5'-fluorescein was used for quantitation of gel bands, and the internal 2-aminopurine was used for stopped-flow analysis of single CMP incorporation. Nucleotide capture parameters were determined by EDTA rapid quench, active-site closure and chemistry were determined by acid quench, and overall nucleotide addition cycle completion was determined using translocation-dependent changes in 2-aminopurine fluorescence. *B*, example EDTA rapid quench data showing starting RNA, +2 "locked" EC, and formation of +3 species over time at a single CTP concentration. Concentration dependence of observed rates at all eight CTP concentrations tested is shown below. *C*, Example acid-quench data at a single CTP concentration with rate concentration dependence plot shown below. For both *B* and *C*, note that there is a minor impurity band running above the starting and +2 RNA species bands, and this was corrected for in the data analysis by subtracting a value corresponding to 4% of the observed +2 band intensity. *D*, fluorescence trace for an example CTP titration series and the corresponding rate concentration dependence plot.

Table 2

Kinetic parameters of thumb-exchanged polymerases

3D ^{pol}	Nucleotide capture EDTA quench			Active-site closure and chemistry acid quench			Complete catalytic cycle stopped flow		
	Catalytic efficiency $\mu M^{-1} s^{-1}$	k_{EDTA} s^{-1}	K_m μM	Catalytic efficiency $\mu M^{-1} s^{-1}$	k_{acid} s^{-1}	K_m μM	Catalytic efficiency $\mu M^{-1} s^{-1}$	k_{2AP} s^{-1}	K_m μM
PPPP	1.8 ± 0.2	56 ± 3	31 ± 4	0.94 ± 0.08	42 ± 2	44 ± 5	0.81 ± 0.11	41 ± 4	50 ± 8
PPPC	1.5 ± 0.1	56 ± 2	38 ± 3	0.67 ± 0.07	37 ± 3	55 ± 7	0.59 ± 0.07	31 ± 3	53 ± 8
CCCP	1.1 ± 0.1	60 ± 4	57 ± 6	0.56 ± 0.02	37 ± 1	14 ± 1	0.65 ± 0.12	38 ± 5	59 ± 13
CCCC	1.1 ± 0.1	59 ± 5	56 ± 8	0.57 ± 0.07	35 ± 3	51 ± 4	0.56 ± 0.09	33 ± 4	59 ± 10

construct to make its coxsackievirus thumb more polio-like. These T447L_{CV} and A450E_{CV} surface mutations effectively restore the poliovirus Leu⁴⁴⁶ and Glu⁴⁴⁹ residues involved in the 3D^{pol}–3D^{pol} interface, resulting in mutant chimeric polymerases we call PPPC_m (Fig. 7B). Interestingly, introducing these two mutations restored virus growth, resulting in small-plaque phenotype viruses that titered at near WT levels after one passage in HeLa cells. We recovered viruses with the thumb domain exchange starting before (PPPC_{lm}) and after (PPPC_{sm}) the 3D^{pol} motif E primer grip region, indicating that this element can also be exchanged between viruses. In an attempt to recover spontaneous mutations that could further enhance virus growth, we carried out 10 serial blind passages of viruses containing mutated coxsackievirus thumb domains under conditions that would potentially select for more rapidly replicating viruses. However, the resulting PPPC_{sm} and PPPC_{lm} viruses retained small plaque phenotypes and were indistinguishable from P₁ viruses. Sequencing of 30 TOPO-TA clones for each virus also failed to show any minor population variants or additional mutations in either 3D^{pol} or 3C^{pro} coding regions.

Several chimeras were nonviable (NV) following initial transfections and infections, because no plaques were detected at P₀ and P₁ (Fig. 7, A and B). After 10 cycles of passage, neither CPE nor plaques were observed for the following NV chimeras: PPPCs, PPPC_l, CCCP, PPCC, PCCC, and CCCC. cDNA also failed to yield PCR products, indicating that neither cytopathic nor noncytopathic virus were present (38). These data reinforce other studies of interspecies incompatibility when swapping enterovirus B and C polymerases (39). Notably, T447L_{CV} and A450E_{CV} mutations in the CV thumb domain of PPPC chimeras overcome one aspect of this interspecies incompatibility (Fig. 7, PPPC_{sm} and PPPC_{lm}).

Discussion

The picornaviral 3D^{pol} enzymes are generally considered the smallest viral polymerases and their core structure composed of palm, fingers, and thumb domains is highly conserved at the structural level despite sequence divergence (1, 9, 35, 40, 41). Structures of polymerases alone and their complexes with RNA have provided insights into the molecular architecture and mechanisms of the elongation complex, including the RNA path through the enzyme and the existence of a unique palm domain–based active-site closure mechanism that can be used to fine-tune replication fidelity. In the study presented here we use poliovirus and coxsackievirus B3 polymerases, two enzymes with inherently different elongation rates and nucleotide discrimination factors (23), to examine the extent to which differ-

ent biochemical functions could be assigned to modular 3D^{pol} structural domains.

Pinky finger controls RNA binding

Initiation, measured as a combination of slow RNA binding followed by the faster first nucleotide addition, is primarily controlled by the pinky finger because exchanging this structural element between the two polymerases almost perfectly reverses their initiation times. From a structural perspective, the pinky finger forms the outer wall of the template RNA channel and it contacts the RNA both before and after the active site. Notably, the pinky finger contains the polymerase motif G sequence within residues 109–118 that (i) fold into the major groove of the nascent duplex, (ii) interact with the single-stranded template backbone via residues 114 and 115 that are opposite the +2 nucleotide-binding pocket, and (iii) ends with Tyr¹¹⁸ located at the opening of a putative extended RNA entry channel (42). Folded above motif G, there is an extended conformation for residues 124–139 that includes Arg¹²⁸ and Lys¹³³, both of which contact product-strand phosphate groups, and Lys¹²⁷, which interacts with a template-strand phosphate. This latter interaction is interesting because it is stabilized by an intricate protein fold wherein motif G residues wrap around the aliphatic portion of the Lys¹²⁷ side chain to position its NH₃⁺ group for an electrostatic contact with the template-strand phosphate of the priming base pair. As such, this is a direct link between proper folding of the pinky finger and structural interactions that recognize and/or position the RNA in the active site. The Lys¹²⁷ residue is conserved in enteroviruses, and there is rapid reversion of an introduced K127A mutation, indicating the lysine is required for poliovirus replication (42). The pinky finger also contains a conserved *cis*-Pro¹¹⁹ flanked by conserved Gly¹¹⁷ and Gly¹²⁴ residues in a folding motif that may be poised for conformational changes via proline *cis/trans*-isomerization (41), and a G117A mutation results in complete loss of electron density for residues 112–129, suggesting cooperative folding within the pinky finger (43).

Based on this, we propose that motions and folding transitions within the pinky finger open the polymerase for template loading and then lock the RNA into place for processive elongation. The pinky finger folding does not require the presence of nucleic acid, as shown by essentially identical conformations in the absence and presence of RNA for multiple picornaviral polymerases (1, 3). Initiation kinetics could thus be governed by either the rate of pinky unfolding to open the template RNA channel or by the rate of pinky refolding to lock the RNA in place. We do not yet know which of these events explains the different rates of the PV and CV pinky fingers but suspect the

Modular functions of picornavirus polymerase domains

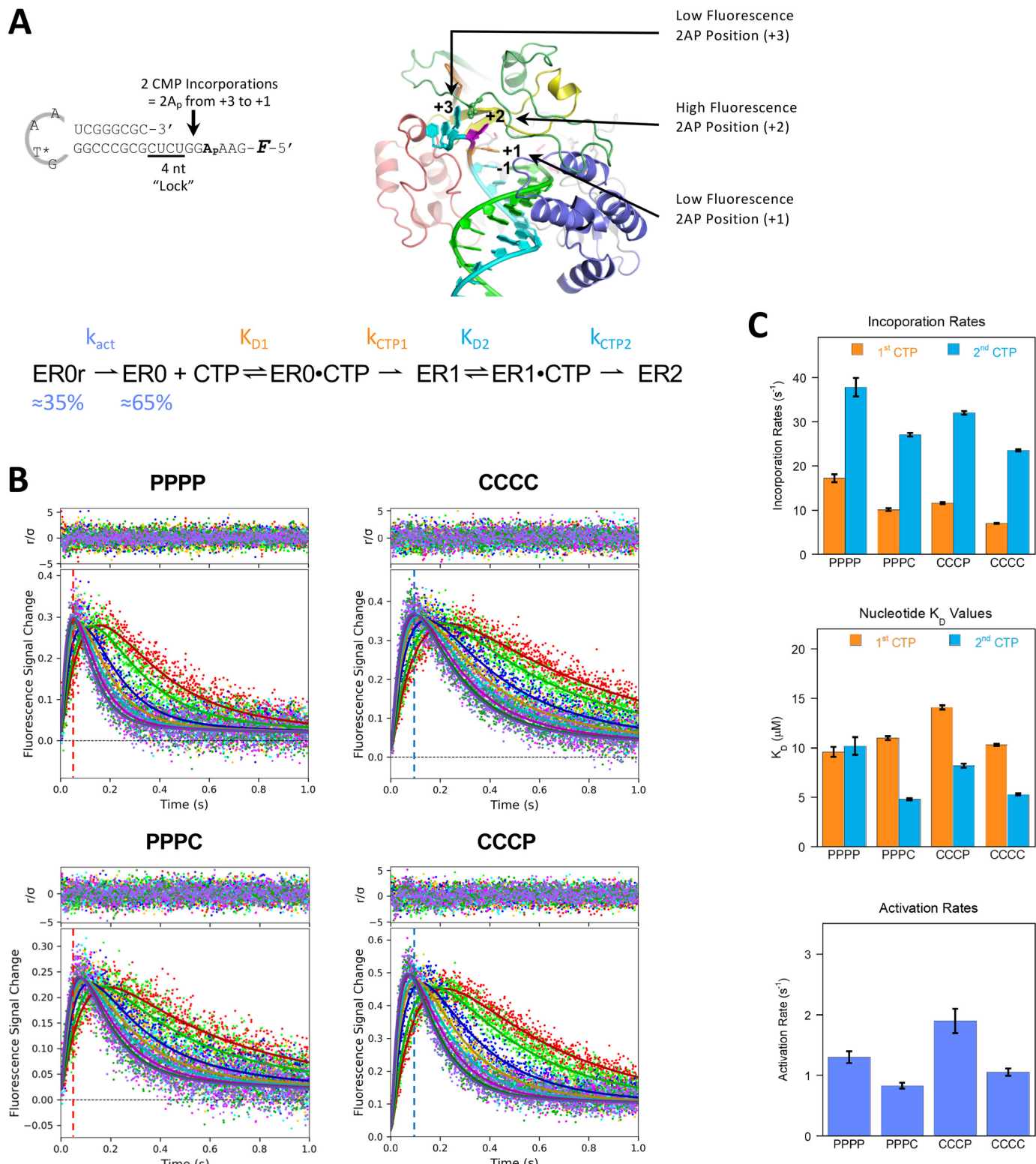


Figure 6. Kinetic modeling of double CMP incorporation reaction. **A**, RNA construct used for two CMP incorporation steps studied by stopped-flow 2-aminopurine fluorescence. The elongation complex structure shows the different environments for the 2-aminopurine as it is translocated from the +3 to the +2 site and then to the +1 site after the two CMP incorporation cycles. **B**, kinetic model used for analysis by global fitting in the program Kintek Explorer. Each nucleotide addition cycle incorporation step is fitted to a CTP dissociation constant (K_{D1} and K_{D2}) and an elongation rate constant (k_{CTP1} , k_{CTP2}), and a slow activation step (k_{act}) is used to account for ~35% of the 20 nm total locked elongation complexes being in a relaxed state (ER0r) at the beginning of the stopped-flow time course (see text). **B**, fluorescence traces showing raw data with simulated traces and associated residuals from the fitted kinetic model for the two WT (PPPP and CCCC) and thumb-exchanged (PPPC and CCCP) polymerases. The data were collected at eight different CTP concentrations, the curves reflect KinTek Explorer model obtained by a global fit of the data, residuals are shown above each data plot, and the vertical dashed lines are visual aids that reflect the time position of peak fluorescence for each WT polymerase (PV in red and CV in blue). **C**, bar graphs showing rate constants for the overall nucleotide addition cycle, CTP K_D values, and activation rates of the four polymerases. Error bars represent standard errors of the parameters obtained from the global fits.

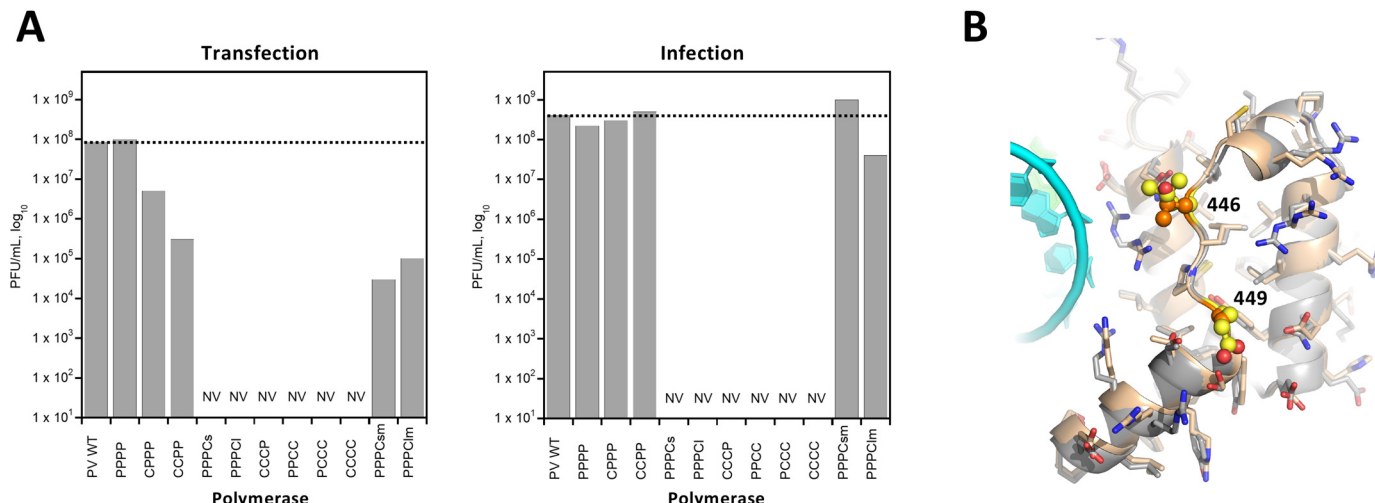


Figure 7. Chimeric virus growth analysis. *A*, viral titers obtained from poliovirus genomes carrying the chimeric polymerases upon RNA transfection (left panel) and subsequent infection (right panel) of cells with chimeric polymerase viruses. Only polymerases containing both the palm and thumb domains from poliovirus were initially viable, but virus was recovered from the short and long thumb exchanges (PPPC_s and PPPC_m) when their coxsackievirus thumbs were mutated to be more poliovirus-like (PPPC_m and PPPC_m). PV WT is a control for the construction of the chimeric polymerase viruses. *B*, structural superposition of the thumb domains from poliovirus (gray) and coxsackievirus (wheat) with the two residues mutated in the two PPPC_m chimeric polymerases shown with atom spheres. These residue pairs are Leu⁴⁴⁶/Asp⁴⁴⁹ in PV (yellow) and Thr⁴⁴⁷/Ala⁴⁵⁰ in CV (orange).

slower initiation rate for PV 3D^{pol} is due to a slow refolding event based on the higher B-factors observed in structures solved in the absence *versus* presence of RNA. Considering the pinky finger as a semi-independent functional unit also makes sense in the context of other RdRP structures: although picornaviral polymerase structures are almost identical, there is a distinct difference in the pinky finger whereby a surface helix composed of residues 128–138 in PV is rotated ~90° in aphtho-, cardio-, and kobuviral polymerases (40, 44). This alternate helix rotation is also seen in noroviral and caliciviral polymerases, whose overall structures are quite similar to the picornaviral ones.

Thumb domain affects translocation

The pinky and full fingers exchanged chimeras both kept the palm and thumb domains together in a polymerase “core,” and the elongation rates and nucleotide discrimination factors cluster according to this core, *i.e.* CPPP and CCPP are polio-like, whereas PCCC and PPCC are coxsackie-like (Fig. 4). It is only when we separate the palm and thumb with the PPPC and CCCP constructs that we get intermediate values for the elongation rates and discrimination factors. To investigate this further, we used a combination of rapid chemical quench and stopped-flow fluorescence experiments (Fig. 5 and Table 2). Data from both the EDTA- and acid-quench experiments show that nucleotide incorporation rates and catalytic efficiencies follow the origin of the palm and fingers domains, whereas the translocation rates follow the origin of the thumb domain.

The EDTA quench experiments reflect the kinetics of NTP capture that ultimately results in product formation, even if subsequent steps needed to do chemistry are slow; once bound to the polymerase, the NTP-Mg²⁺ complex is effectively immune to chelation of its Mg²⁺ ion by EDTA present in the bulk solution. Exchanging the thumb domains does not significantly alter the observed EDTA-quench rates, indicating that

the thumb does not play a major role in the first step of the NAC. Next, acid-quench experiments were used to investigate the rate at which active-site closure and chemistry for +1 product formation occur. Unlike the EDTA quench, this assay immediately stops the reaction through protonation of active-site groups and protein denaturation. The acid-quench rates are slower than the capture step rates because they include the additional molecular motions needed to close the active site and perform chemistry. The PPPC thumb exchange reduced both the rate and catalytic efficiency compared with PPPP, indicating that the thumb domain can exert an indirect effect on the chemistry step. This is likely due to altering the exact positioning and/or motions of the priming ribose in the active site. Last, the 2-aminopurine fluorescence data reports on template translocation, the last step in the NAC. The WT polymerases have k_{2AP} values that are only slightly slower than their k_{acid} rates, indicating that translocation is normally a rapid step following catalysis. In contrast, the thumb exchanges resulted in an almost perfect reversal of the observed rates. The double CMP incorporation data similarly showed that placing the PV thumb onto CV polymerase increased NAC rates by ~40%, and conversely the CV thumb slowed PV polymerase by ~40% (Fig. 6). This two-cycle modeling also showed that for any polymerase, the second nucleotide addition was more efficient than the first, primarily because of 2–3-fold faster incorporation rates. This likely reflects subtle biochemical and dynamics changes in the 3D^{pol}-RNA complex as it transitions to the more processive state of a true elongation complex.

Altogether, these kinetic data are consistent with previous studies showing that active-site closure is the rate-limiting step in the 3D^{pol} catalytic cycle (45). Structures of 3D^{pol} elongation complexes show that this step involves a subtle movement within the palm domain whereby the C-terminal end of motif A moves to fully form the three-stranded β -sheet with motif C and position the active-site aspartates for catalysis (9). This is

Modular functions of picornavirus polymerase domains

associated with movements of motif D, which forms the outer edge of the NTP entry tunnel and interacts tightly with motif A via backbone hydrogen bonding and cofolding (24, 32, 46). All these interactions are within the palm domain, consistent with our data showing that this domain is the primary effector of both the nucleotide-binding and chemistry steps. The new revelation from our thumb-exchanged polymerases is that the thumb domain plays a role in controlling translocation, the final step in the nucleotide addition cycle.

Poliovirus replication studies

In a PV background we recovered viruses with near WT titers for both the CPPP and CCPP polymerases, showing that both the pinky and the full fingers could be exchanged without significant impact on viral replication. We initially did not recover any virus from the thumb-exchanged polymerases, and because of the biochemical coupling between the palm and thumb domains, we tested this with constructs in which the palm–thumb junction point was located either before or after the motif E primer-grip element. However, an alternative explanation for this result can be found in the observation that the poliovirus thumb domain has been implicated in the formation of two different protein–protein interfaces. The first is with the palm of another 3D^{pol} to form long polymerase fibers (47, 48) and sheet-like structures (49–51), and the second is a biochemically identified interaction with the 3C domain of the viral 3CD^{pro} protease to stabilize the viral uridylylation complex (52). To further explore the significance of these interfaces for virus growth, we made the coxsackie thumb of PPPC more polio-like by restoring two PV surface residues, Leu⁴⁴⁶ and Glu⁴⁴⁹ (Fig. 7B). Interestingly, these two mutations resulted in near WT titers of chimeric PPPC_{sm} and PPPC_{lm} viruses, clearly indicating that this region of the thumb-domain surface is essential for poliovirus replication. We further attempted to obtain viruses with improved growth characteristics by serial passaging of the PPPC_{sm} and PPPC_{lm} viruses under conditions that would favor the emergence of variants carrying spontaneous mutations. The locations of such mutations could have validated the importance of either the 3D^{pol}–3D^{pol} or the 3D^{pol}–3CD^{pro} interface, but unfortunately none were obtained.

Conclusions

In this study we used the high similarity of poliovirus and coxsackievirus polymerases to generate chimeric 3D^{pol} enzymes and determine the extent to which different biochemical functions could be assigned to RdRP structural domains. The results showed that the pinky finger plays a key role in initiation, whereas nucleotide discrimination and catalysis are primarily associated with the palm domain, and the thumb domain subtly impacts the translocation step and elongation complex stability. We propose a general model for positive-strand RNA virus polymerases wherein the pinky forms a semi-independent subdomain atop the fingers domain whose folding transitions regulate template strand access to the active site.

Experimental procedures

Chimeric polymerase construction

The pinky finger exchanges, *i.e.* CPPP and PCCC proteins, are a straightforward swap of a single contiguous segment from residues 66–150, which includes all of polymerase motif G. In contrast, the full fingers domain exchange is more complicated because it has five cross-over points with the palm domain, and it forms a structural contact with the top of the thumb. The palm–fingers junction points chosen were based on the palm residues resolved and modeled in the original WT PV 3D^{pol} structure (Protein Data Bank entry 1RDR), in which a crystal packing interaction led to the complete unfolding of the fingers domain (41, 53). Note, however, that residues 27–37 at the tip of the index finger were always matched with the origin of the thumb domain so as to preserve the native fingers–thumb contact (Fig. 1B). For the thumb-domain exchanges, polymerases were made with two different junction points located on either side of motif E, often referred to as the “primer-grip” element in the reverse transcriptase literature. These polymerases are designated with a subscripted “l” for a long thumb exchange that includes motif E (PPPC_l) and a subscripted “s” for a short thumb exchange beginning after motif E (PPPC_s). These two thumb-exchange sites generally provided equivalent results in biochemistry experiments, and data are reported for the long thumb junction point that begins with residue 369_{PV} (370_{CV}) unless explicitly stated.

The chimeric polymerase genes were assembled into a T7-based expression vector with the In-Fusion cloning kit (Clontech) using a combination of PCR products, oligonucleotides, and GeneBloc fragments (IDT Inc., Coralville, IA, USA) as needed, and the final constructs were verified by sequencing. Polymerase expression and purification were carried out as previously described (54), with the final purification step being size-exclusion chromatography into a buffer composed of 5 mM Tris, pH 7, 300 mM NaCl, 2 mM tris-(2-carboxyethyl)-phosphine (TCEP), 20% glycerol.

Initiation and stability

Initiation rates were assayed using 5 μM polymerase, 0.5 μM “10+1_12” RNA (54), and 40 μM GTP at room temperature in 75 mM NaCl, 4 mM MgCl₂, 25 mM HEPES, pH 6.5, and 2 mM TCEP. 1-μl samples were removed at various time points up to 15 min and added to 19 μl of quench buffer containing 50 mM EDTA, 400 mM NaCl, 50 mM HEPES, pH 6.5, and 2 mM TCEP. After the initiation reaction had progressed for 15 min, the assay for the temporal stability of the resulting elongation complexes was begun by adding 10 μl of the initiation reaction to 90 μl of 300 mM NaCl, 4 mM MgCl₂, 50 mM HEPES, pH 6.5, and 2 mM TCEP, wherein the high salt concentration limited further initiation and reinitiation by preventing RNA binding. The amount of competent elongation complex still present in this solution was tested at various points over a 4-h period by removing 5-μl aliquots and mixing them with 5 μl of buffer containing 160 μM each of ATP, GTP, and UTP, followed by a 2-min elongation reaction to produce full-length products before quenching with EDTA. The samples were analyzed by denaturing gel electrophoresis using 20% 19:1 polyacrylamide,

7 M urea, 1× TBE gels. RNA bands were detected using a Li-Cor Odyssey 9120 IR imager system to visualize the IRdye 800RS (Li-Cor Biosciences) label on the RNA tetraloop, as previously described (54). The data were mathematically fit to single exponential equations using Kaleidagraph (Synergy Software) to determine time constants for the increased formation of +1 product in the initiation assay or the decreased formation of +7 chase product in the stability assay.

Enzyme kinetics assays

Stopped-flow fluorescence methods were used to measure kinetics of processive elongation (31) and single-nucleotide incorporation (32). Stalled elongation complexes were first generated by incubating 15 μ M polymerase with 10 μ M RNA in 75 mM NaCl, 4 mM MgCl₂, 25 mM HEPES, pH 6.5, 2 mM TCEP, and 60 μ M each of ATP and GTP for 15 min. The resulting complexes were diluted 200-fold to a final RNA concentration of 50 nM with 50 mM HEPES, pH 7, 75 mM NaCl, and 4 mM MgCl₂, generating the sample that was loaded into the stopped-flow instrument and then further diluted 2-fold (final concentration, 25 nM) when mixed with either only CTP or all four NTPs in the reaction cell. MgCl₂ was always maintained at 4 mM excess over the total NTP concentration, and for the processive elongation assays the four NTPs were present at equimolar concentrations. Kinetics data were collected at 30 °C using a Bio-Logic SFM-4000 titrating stopped-flow instrument with a MOS-500 spectrometer. Fluorescence data from the single CMP incorporation and processive elongation reactions were fit using Kaleidagraph (Synergy Software, Reading, PA), and data from double CMP incorporation reactions were analyzed and modeled using KinTek Explorer (Kin-Tek Corp, Austin, TX, USA) (36, 37).

Rapid chemical quench experiments were done by first forming stalled elongation complexes with 15 μ M polymerase and 10 μ M 5'-fluorescein-labeled RNA for 15 min at room temperature in buffer containing 75 mM NaCl, 4 mM MgCl₂, 25 mM HEPES, pH 6.5, 2 mM TCEP, 200 μ M ATP, and 60 μ M GTP. The resulting complexes were diluted 20-fold to a final concentration of 500 nM RNA with reaction buffer consisting of 50 mM HEPES, pH 7, 75 mM NaCl, and 4 mM MgCl₂. Polymerase complexes were further diluted 2-fold in the Bio-Logic QFM-4000 instrument when mixed with various concentrations of CTP, the single-nucleotide substrate, made up in this same buffer. The QFM-4000 instrument controls reaction time by varying flow rate through a 3- μ l reaction chamber that ends at mixing with the quench solution. Stalled elongation complex and CTP were mixed and allowed to react for times ranging from 5 to 2000 ms before quenching with either 300 mM EDTA (final concentration, 100 mM) or 3 M HCl (final concentration, 1 M). A total of 15 μ l of each component was used in the reaction, yielding 45- μ l final sample volumes. For the acid quench, 30 μ l of the final sample was manually added to 30 μ l of 1 M NaOH, 300 mM MES so as to neutralize the samples prior to gel analysis. The reaction products were analyzed by denaturing gel electrophoresis on 20% polyacrylamide (19:1), 7 M urea, 1× TBE gels, and imaged using the 488-nm channel of an Amersham Biosciences Typhoon Imager. Product formation rates were meas-

ured at eight different CTP concentrations with 8–12 time points collected for each concentration. Gel bands were quantified using the program PeakFit (Systat Software) to analyze lane scans by fitting band profiles to Gaussian peaks and closely spaced peaks in a given lane used a common (fitted) peak width to improve quantitation of weak bands. We verified that the 5'-fluorescein modification (56-FAM from IDT Technologies, Inc.) was chemically resistant to the acid-quench conditions.

Virus replication studies

The chimeric polymerases were cloned into the full-length infectious poliovirus cDNA using the In-Fusion method (Clontech) with PCR products, and proper insertion was verified by sequencing. RNA was transcribed from MluI-linearized plasmids using T7 RNA polymerase (Ampliscribe T7 high-yield transcription kit; CellScript Inc.), and 1 μ g was transfected in triplicate into \sim 10⁶ HeLa cells in 35-mm 6-well plates using Transmessenger transfection reagent (Qiagen) according to the manufacturer's instructions. Transfected cells were fed with 2 ml of cell culture medium (Dulbecco's modified Eagle's medium containing 10% fetal bovine serum, 100 units/ml penicillin, and 100 μ g/ml streptomycin) and incubated at 37 °C. The cells were examined for cytopathic effect (CPE) at 24, 48, 72, and 96 h post-transfection. Infectious virus (P₀, passage zero) was harvested following three rounds of freeze-thaw at the time of CPE (or 96 hours post transfection when CPE was absent) and quantified by plaque assay. P₀ virus was then used to infect \sim 10⁷ HeLa cells in T₇₅ flasks at a multiplicity of infection of 10 PFU/cell. Infected cells were incubated with 12 ml of cell culture medium. P₁ virus was harvested by freeze-thawing cells at 24–72 h postinfection (hpi), based on the timing of cytopathic effects, and quantified by plaque assay.

The P₁ virus RNA genomes were analyzed to verify the presence and integrity of the chimeric polymerase constructs. P₁ virus (8 ml) was layered onto 3 ml of 30% (w/v) sucrose in PBS followed by centrifugation at 36,000 rpm for 4 h at 4 °C using a Beckman SW41 rotor. Pelleted material containing virus was resuspended in 400 μ l of 0.5% SDS buffer (0.5% SDS, 10 mM Tris-HCl, pH 7.5, and 100 mM NaCl). Virion RNA was isolated by phenol:chloroform:isoamyl alcohol extraction and ethanol precipitation. Virion RNA was solubilized in 10 μ l of water. cDNA was synthesized using 2 μ l of virion RNA in 20- μ l reactions using Superscript III (Invitrogen) reverse transcriptase and a primer complementary to poliovirus nucleotides 7415–7440 in the 3' NTR (nucleotides 7440–7415, 5'-CTCCGAATTAAAGAAAAATTACCCC-3'). The reactions were incubated at 65 °C for 5 min, followed by the addition of RT, followed by further incubation at 55 °C for 1 h and 70 °C for 15 min. cDNA corresponding to the 3CD region of poliovirus RNA was amplified using the following primers: forward primer (nucleotides 5816–5838), 5'-CTC GGT GGG CGC CAA ACT GCT CG-3'; and reverse primer (nucleotides 7415–7740), 5'-CTC CGA ATT AAA GAA AAA TTT ACC CC-3'.

PCRs (50 μ l) containing 2 μ l of viral cDNA were incubated for 2 min at 95 °C and subjected to 30 cycles of PCR (94 °C for 30 s, 60 °C for 30 s, and 72 °C for 2 min) and a final extension at 72 °C for 2 min. PCR products were analyzed by agarose gel

Modular functions of picornavirus polymerase domains

electrophoresis and ethidium bromide staining. Plasmid DNAs and viral cDNAs (~3 µl of PCR products – ExoSAP treated) were sequenced using the forward and reverse primers noted above in the University of Colorado Cancer Center DNA Sequencing Core Laboratory.

Serial passage of PPPC viruses

Viruses containing the two mutated thumb-exchanged polymerases, PPPC_{sm} and PPPC_{lm}, exhibited a small plaque phenotype, and serial passage in HeLa cells was used to see whether both the genotypes and phenotypes of these viruses were stable. ~10⁷ HeLa cells in T₇₅ flasks were infected with 1 ml of P₁ progeny virus (a multiplicity of infection of ~10 PFU/cell). The virus was harvested at 24 hpi by three rounds of freeze–thaw in 10 ml of culture medium. After 10 cycles of infection, plaque assays were used to examine viral titers and plaque phenotypes, and viral cDNA was prepared as described above. Viral cDNA was sequenced both before and after TOPO-TA cloning. 30 TOPO-TA clones were sequenced in the 3CD region of the genome to look for individual variants within the population. PPPC_{sm} and PPPC_{lm} viruses retained small plaque phenotypes after 10 cycles of infection and were indistinguishable from P₁ viruses. No mutations were detected in PPPC_{sm} and PPPC_{lm} viruses after 10 cycles of infection beyond those engineered into each virus.

Serial passage of nonviable chimeras

Several chimeras were not viable following initial transfections and infections because no plaques were detected at P₀ and P₁. For these NV chimeras (PPPC_s, PPPC_b, CCCP, PPCC, PCCC, and CCCC), we used serial passage in HeLa cells to see whether viable virus would arise during passage. Undiluted P₀ was used to inoculate ~10⁷ HeLa cells in T₇₅ flasks. The cells were monitored by microscopy for CPE. At 96 hpi, the cells were subjected to three rounds of freeze–thaw in 10 ml of culture medium. After 10 cycles of serial passage, plaque assays were used to detect virus, and cDNA was prepared from medium concentrated by centrifugation as described above. Throughout serial passage, neither CPE nor plaques were observed for these NV chimeras (PPPC_s, PPPC_b, CCCP, PPCC, PCCC, and CCCC), and cDNA failed to yield PCR products, indicating that neither cytopathic nor noncytopathic virus were present (38).

Data availability

All data are presented and described in the article.

Acknowledgments—We thank Grace Campagnola and Emily Gervais for general assistance and feedback on the project.

Author contributions—C. L. W., B. J. K., and S. B. data curation; C. L. W., B. J. K., and S. B. formal analysis; C. L. W. validation; C. L. W., B. J. K., and S. B. investigation; C. L. W., B. J. K., and S. B. methodology; C. L. W., B. J. K., and D. J. B. writing-original draft; D. J. B. and O. B. P. conceptualization; D. J. B. supervision; D. J. B. and O. B. P. funding acquisition; D. J. B. and O. B. P. project administration; O. B. P. writing-review and editing.

Funding and additional information—This work was supported by National Institutes of Health Grants AI059130 (to O. B. P.) and AI042189 (to D. J. B.). The content is solely the responsibility of the authors and does not necessarily represent the official views of the National Institutes of Health.

Conflict of interest—The authors declare that they have no conflicts of interest with the contents of this article.

Abbreviations—The abbreviations used are: RdRP, RNA-dependent RNA polymerase; PV, poliovirus; CV, coxsackievirus B3; dCTP, 2'-deoxy-CTP; NAC, nucleotide addition cycle; PFU, plaque-forming unit; NV, nonviable; TCEP, tris-(2-carboxyethyl)-phosphine; CPE, cytopathic effect; hpi, h postinfection; 2AP, 2-aminopurine.

References

1. Peersen, O. B. (2017) Picornaviral polymerase structure, function, and fidelity modulation. *Virus Res.* **234**, 4–20 [CrossRef](#) [Medline](#)
2. Ferrero, D., Ferrer-Orta, C., and Verdaguera, N. (2018) Viral RNA-dependent RNA polymerases: a structural overview. *Subcell. Biochem.* **88**, 39–71 [CrossRef](#) [Medline](#)
3. Peersen, O. B. (2019) A comprehensive superposition of viral polymerase structures. *Viruses* **11**, 745 [CrossRef](#) [Medline](#)
4. Steitz, T. A. (1998) A mechanism for all polymerases. *Nature* **391**, 231–232 [CrossRef](#) [Medline](#)
5. Thompson, A. A., Albertini, R. A., and Peersen, O. B. (2007) Stabilization of poliovirus polymerase by NTP binding and fingers–thumb interactions. *J. Mol. Biol.* **366**, 1459–1474 [CrossRef](#) [Medline](#)
6. Steitz, T. A. (2006) Visualizing polynucleotide polymerase machines at work. *EMBO J.* **25**, 3458–3468 [CrossRef](#) [Medline](#)
7. Temiakov, D., Patlan, V., Anikin, M., McAllister, W. T., Yokoyama, S., and Vassylyev, D. G. (2004) Structural basis for substrate selection by t7 RNA polymerase. *Cell* **116**, 381–391 [CrossRef](#) [Medline](#)
8. Yin, Y. W., and Steitz, T. A. (2004) The structural mechanism of translocation and helicase activity in T7 RNA polymerase. *Cell* **116**, 393–404 [CrossRef](#) [Medline](#)
9. Gong, P., and Peersen, O. B. (2010) Structural basis for active site closure by the poliovirus RNA-dependent RNA polymerase. *Proc. Natl. Acad. Sci. U.S.A.* **107**, 22505–22510 [CrossRef](#) [Medline](#)
10. Wu, J., and Gong, P. (2018) Visualizing the nucleotide addition cycle of viral RNA-dependent RNA polymerase. *Viruses* **10**, 24 [CrossRef](#) [Medline](#)
11. Shu, B., and Gong, P. (2016) Structural basis of viral RNA-dependent RNA polymerase catalysis and translocation. *Proc. Natl. Acad. Sci. U.S.A.* **113**, E4005–E4014 [CrossRef](#) [Medline](#)
12. Korboukh, V. K., Lee, C. A., Acevedo, A., Vignuzzi, M., Xiao, Y., Arnold, J. J., Hemperly, S., Graci, J. D., August, A., Andino, R., and Cameron, C. E. (2014) RNA virus population diversity: an optimum for maximal fitness and virulence. *J. Biol. Chem.* **289**, 2931–2954 [CrossRef](#)
13. Andino, R., and Domingo, E. (2015) Viral quasispecies. *Virology* **479–480**, 46–51 [CrossRef](#) [Medline](#)
14. Lauring, A. S., and Andino, R. (2010) Quasispecies theory and the behavior of RNA viruses. *PLoS Pathogens* **6**, e1001005 [CrossRef](#) [Medline](#)
15. McCrone, J. T., and Lauring, A. S. (2018) Genetic bottlenecks in intraspecies virus transmission. *Curr. Opin. Virol.* **28**, 20–25 [CrossRef](#) [Medline](#)
16. Gnädig, N. F., Beaucourt, S., Campagnola, G., Bordería, A. V., Sanz-Ramos, M., Gong, P., Blanc, H., Peersen, O. B., and Vignuzzi, M. (2012) Coxsackievirus B3 mutator strains are attenuated *in vivo*. *Proc. Natl. Acad. Sci. U.S.A.* **109**, E2294–E2303 [CrossRef](#) [Medline](#)
17. Pfeiffer, J. K., and Kirkegaard, K. (2003) A single mutation in poliovirus RNA-dependent RNA polymerase confers resistance to mutagenic nucleotide analogs via increased fidelity. *Proc. Natl. Acad. Sci. U.S.A.* **100**, 7289–7294 [CrossRef](#) [Medline](#)
18. Peck, K. M., and Lauring, A. S. (2018) Complexities of viral mutation rates. *J. Virol.* **92**, e01031–17 [CrossRef](#) [Medline](#)

19. Kempf, B. J., Peersen, O. B., and Barton, D. J. (2016) Poliovirus polymerase Leu420 facilitates RNA recombination and ribavirin resistance. *J. Virol.* **90**, 8410–8421 [CrossRef](#) [Medline](#)
20. Xiao, Y., Rouzine, I. M., Bianco, S., Acevedo, A., Goldstein, E. F., Farkov, M., Brodsky, L., and Andino, R. (2016) RNA recombination enhances adaptability and is required for virus spread and virulence. *Cell Host Microbe* **19**, 493–503 [CrossRef](#) [Medline](#)
21. Woodman, A., Lee, K. M., Janissen, R., Gong, Y. N., Dekker, N. H., Shih, S. R., and Cameron, C. E. (2019) Predicting intraserotypic recombination in enterovirus 71. *J. Virol.* **93**, e02057-18 [CrossRef](#) [Medline](#)
22. Kempf, B. J., Watkins, C. L., Peersen, O. B., and Barton, D. J. (2019) Picornavirus RNA recombination counteracts error catastrophe. *J. Virol.* **93**, [CrossRef](#) [Medline](#)
23. Campagnola, G., McDonald, S., Beaumont, S., Vignuzzi, M., and Peersen, O. B. (2015) Structure–function relationships underlying the replication fidelity of viral RNA-dependent RNA polymerases. *J. Virol.* **89**, 275–286 [CrossRef](#) [Medline](#)
24. Yang, X., Smidansky, E. D., Maksimchuk, K. R., Lum, D., Welch, J. L., Arnold, J. J., Cameron, C. E., and Boehr, D. D. (2012) Motif D of viral RNA-dependent RNA polymerases determines efficiency and fidelity of nucleotide addition. *Structure* **20**, 1519–1527 [CrossRef](#) [Medline](#)
25. Moustafa, I. M., Korboukh, V. K., Arnold, J. J., Smidansky, E. D., Marcotte, L. L., Gohara, D. W., Yang, X., Sánchez-Farrán, M. A., Filman, D., Maranas, J. K., Boehr, D. D., Hogle, J. M., Colina, C. M., and Cameron, C. E. (2014) Structural dynamics as a contributor to error-prone replication by an RNA-dependent RNA polymerase. *J. Biol. Chem.* **289**, 36229–36248 [CrossRef](#) [Medline](#)
26. Shi, J., Perryman, J. M., Yang, X., Liu, X., Musser, D. M., Boehr, A. K., Moustafa, I. M., Arnold, J. J., Cameron, C. E., and Boehr, D. D. (2019) Rational control of poliovirus RNA-dependent RNA polymerase fidelity by modulating motif-D loop conformational dynamics. *Biochemistry* **58**, 3735–3743 [CrossRef](#) [Medline](#)
27. Yang, X., Welch, J. L., Arnold, J. J., and Boehr, D. D. (2010) Long-range interaction networks in the function and fidelity of poliovirus RNA-dependent RNA polymerase studied by nuclear magnetic resonance. *Biochemistry* **49**, 9361–9371 [CrossRef](#) [Medline](#)
28. Cameron, C. E., Moustafa, I. M., and Arnold, J. J. (2009) Dynamics: the missing link between structure and function of the viral RNA-dependent RNA polymerase?. *Curr. Opin. Struct. Biol.* **19**, 768–774 [CrossRef](#) [Medline](#)
29. Cornell, C. T., and Semler, B. L. (2002) Subdomain specific functions of the RNA polymerase region of poliovirus 3CD polyprotein. *Virology* **298**, 200–213 [CrossRef](#) [Medline](#)
30. Peersen, O. (2019) Polymerase structure alignments. [CrossRef](#)
31. Gong, P., Campagnola, G., and Peersen, O. B. (2009) A quantitative stopped-flow fluorescence assay for measuring polymerase elongation rates. *Anal. Biochem.* **391**, 45–55 [CrossRef](#) [Medline](#)
32. McDonald, S., Block, A., Beaumont, S., Moratorio, G., Vignuzzi, M., and Peersen, O. B. (2016) Design of a genetically stable high fidelity coxsackievirus B3 polymerase that attenuates virus growth *in vivo*. *J. Biol. Chem.* **291**, 13999–14011 [CrossRef](#) [Medline](#)
33. Karr, J. P., and Peersen, O. B. (2016) ATP is an allosteric inhibitor of coxsackievirus B3 polymerase. *Biochemistry* **55**, 3995–4002 [CrossRef](#) [Medline](#)
34. Arnold, J. J., and Cameron, C. E. (2000) Poliovirus RNA-dependent RNA polymerase (3Dpol): assembly of stable, elongation-competent complexes by using a symmetrical primer-template substrate (sym/sub). *J. Biol. Chem.* **275**, 5329–5336 [CrossRef](#) [Medline](#)
35. Gong, P., Kortus, M. G., Nix, J. C., Davis, R. E., and Peersen, O. B. (2013) Structures of coxsackievirus, rhinovirus, and poliovirus polymerase elongation complexes solved by engineering RNA mediated crystal contacts. *PLoS One* **8**, e60272 [CrossRef](#) [Medline](#)
36. Johnson, K. A., Simpson, Z. B., and Blom, T. (2009) Global kinetic explorer: a new computer program for dynamic simulation and fitting of kinetic data. *Anal. Biochem.* **387**, 20–29 [CrossRef](#) [Medline](#)
37. Johnson, K. A., Simpson, Z. B., and Blom, T. (2009) FitSpace explorer: an algorithm to evaluate multidimensional parameter space in fitting kinetic data. *Anal. Biochem.* **387**, 30–41 [CrossRef](#) [Medline](#)
38. Smithee, S., Tracy, S., and Chapman, N. M. (2015) Mutational disruption of cis-acting replication element 2C in coxsackievirus B3 leads to 5'-terminal genomic deletions. *J. Virol.* **89**, 11761–11772 [CrossRef](#) [Medline](#)
39. Bell, Y. C., Semler, B. L., and Ehrenfeld, E. (1999) Requirements for RNA replication of a poliovirus replicon by coxsackievirus B3 RNA polymerase. *J. Virol.* **73**, 9413–9421 [CrossRef](#) [Medline](#)
40. Dubankova, A., Horova, V., Klíma, M., and Boura, E. (2019) Structures of kobuviral and sainiviral polymerases reveal conserved mechanism of picornaviral polymerase activation. *J. Struct. Biol.* **208**, 92–98 [CrossRef](#) [Medline](#)
41. Thompson, A. A., and Peersen, O. B. (2004) Structural basis for proteolysis-dependent activation of the poliovirus RNA-dependent RNA polymerase. *EMBO J.* **23**, 3462–3471 [CrossRef](#) [Medline](#)
42. Kortus, M. G., Kempf, B. J., Haworth, K. G., Barton, D. J., and Peersen, O. B. (2012) A template RNA entry channel in the fingers domain of the poliovirus polymerase. *J. Mol. Biol.* **417**, 263–278 [CrossRef](#) [Medline](#)
43. Thompson, A. A. (2006) X-ray Crystal Structure and Biophysical Analysis of the Poliovirus RNA-dependent RNA Polymerase, Ph.D. thesis, Colorado State University, Fort Collins, CO
44. Ferrer-Orta, C., Arias, A., Perez-Luque, R., Escarmís, C., Domingo, E., and Verdaguera, N. (2004) Structure of foot-and-mouth disease virus RNA-dependent RNA polymerase and its complex with a template-primer RNA. *J. Biol. Chem.* **279**, 47212–47221 [CrossRef](#) [Medline](#)
45. Arnold, J. J., and Cameron, C. E. (2004) Poliovirus RNA-dependent RNA polymerase (3Dpol): pre-steady-state kinetic analysis of ribonucleotide incorporation in the presence of Mg²⁺. *Biochemistry* **43**, 5126–5137 [CrossRef](#) [Medline](#)
46. Shen, H., Sun, H., and Li, G. (2012) What is the role of motif D in the nucleotide incorporation catalyzed by the RNA-dependent RNA polymerase from poliovirus?. *PLoS Comput. Biol.* **8**, e1002851 [CrossRef](#) [Medline](#)
47. Hobson, S. D., Rosenblum, E. S., Richards, O. C., Richmond, K., Kirkegaard, K., and Schultz, S. C. (2001) Oligomeric structures of poliovirus polymerase are important for function. *EMBO J.* **20**, 1153–1163 [CrossRef](#) [Medline](#)
48. Spagnolo, J. F., Rossignol, E., Bullitt, E., and Kirkegaard, K. (2010) Enzymatic and nonenzymatic functions of viral RNA-dependent RNA polymerases within oligomeric arrays. *RNA* **16**, 382–393 [CrossRef](#) [Medline](#)
49. Lyle, J. M., Bullitt, E., Bienz, K., and Kirkegaard, K. (2002) Visualization and functional analysis of RNA-dependent RNA polymerase lattices. *Science* **296**, 2218–2222 [CrossRef](#) [Medline](#)
50. Tellez, A. B., Wang, J., Tanner, E. J., Spagnolo, J. F., Kirkegaard, K., and Bullitt, E. (2011) Interstitial contacts in an RNA-dependent RNA polymerase lattice. *J. Mol. Biol.* **412**, 737–750 [CrossRef](#) [Medline](#)
51. Wang, J., Lyle, J. M., and Bullitt, E. (2013) Surface for catalysis by poliovirus RNA-dependent RNA polymerase. *J. Mol. Biol.* **425**, 2529–2540 [CrossRef](#) [Medline](#)
52. Shen, M., Reitman, Z. J., Zhao, Y., Moustafa, I., Wang, Q., Arnold, J. J., Pathak, H. B., and Cameron, C. E. (2008) Picornavirus genome replication. Identification of the surface of the poliovirus (PV) 3C dimer that interacts with PV 3Dpol during VPg uridylylation and construction of a structural model for the PV 3C2-3Dpol complex. *J. Biol. Chem.* **283**, 875–888 [CrossRef](#) [Medline](#)
53. Hansen, J. L., Long, A. M., and Schultz, S. C. (1997) Structure of the RNA-dependent RNA polymerase of poliovirus. *Structure* **5**, 1109–1122 [CrossRef](#) [Medline](#)
54. Hobday, S. E., Kempf, B. J., Steil, B. P., Barton, D. J., and Peersen, O. B. (2010) Poliovirus polymerase residue 5 plays a critical role in elongation complex stability. *J. Virol.* **84**, 8072–8084 [CrossRef](#) [Medline](#)